Report Date: April 1, 2003

Semi-Annual Technical Progress Report

INVESTIGATION OF EFFICIENCY IMPROVEMENTS DURING CO_2 INJECTION IN HYDRAULICALLY AND NATURALLY FRACTURED RESERVOIRS

DOE Contract No.: DE-FC26-01BC15361

Harold Vance Department of Petroleum Engineering
Texas A& M University
3116 TAMU
College Station, TX 77843-3116
(979) 845-2241

Contract Date:	September 1, 2001
Anticipated Completion Date:	September 1, 2003
Principal Investigator:	David S. Schechter Harold Vance Department of Petroleum Engineering
Contracting Officer's Representative:	Dan Ferguson National Petroleum Technology Office
Report Period:	September 27, 2002- March 27, 2003

DISCLAIMER

ABSTRACT

The objective of this project is to perform unique laboratory experiments with artificial fractured cores (AFCs) and X-ray CT to examine the physical mechanisms of bypassing in HFR and NFR that eventually result in less efficient CO_2 flooding in heterogeneous or fracture-dominated reservoirs. This report provides results of the third semi-annual technical progress report that consists of application of X-Ray Tomography results to validate our numerical modeling of flow in fractures.

Spontaneous imbibition plays a very important role in the displacement mechanism of non-wetting fluid in naturally fractured reservoirs. To quantify this spontaneous imbibition process, we developed a 2D two-phase numerical model. This numerical model was developed because an available commercial simulator cannot be used to model small-scale experiments with different boundary conditions. In building the numerical model, we started with the basic equation of fluid flow and developed a numerical approach of solving the non-linear diffusion saturation equation. We compared our numerical model with the analytical solution of this equation to ascertain the limitations of the assumptions used to arrive at that solution. The unique aspect of this paper is that we validated our model with X-ray computerized tomography (CT) experimental data from a different spontaneous imbibition experiment, where two simultaneously varying parameters of weight gain and CT water saturation were used. This requires us to undertake extensive sensitivity studies on key parameters before a successful match could be obtained. We also successfully captured our own X-ray computerized tomography (CT) laboratory experiment on a fractured core.

TABLE OF CONTENTS

LIST OF TABLES

LIST OF FIGURES

I. X-Ray Tomography Results Validate Numerical Modeling of Flow in Fractures

1.1 Introduction

The quest to produce more oil has led various researchers to evaluate more complex reservoirs such as naturally fractured ones. The complexity of fluid flow in these types of reservoirs arises from the fact that there are two media, which can allow fluids to flow through them. This leads to the logical conclusion that there are two principal media of fluid flow. The first is through the porous medium called the matrix flow and the other is the flow through the fracture network. At the heart of this phenomenon lies the problem of interaction of these two flow media with each other. In naturally fractured reservoirs the matrix acts as a source where hydrocarbons are present whereas the fractures facilitate in fast recovery of these hydrocarbons. Hence it is important to study what makes the matrix produce more oil. Water is used as a means to efficiently displace oil. But fluid flow in porous media, which is determined primarily by capillary force, is relatively difficult phenomenon to quantify and there has been much research effort directed in this direction like that of Handy[2], Garg *et al.*[3], Babadagli and Ershaghi[4], Li and Horne[5], Akin and Kovscek[6], Reis and Cil[7], Zhou *et al.*[8], to name a few. Also, depending on the geometry of the fracture, there may or may not be any capillary force in the fracture network. This force is responsible for imparting the spontaneity to fluid flow within naturally fractured reservoirs. Given the complexity of quantifying the spread of fractures, it is even difficult to ascertain the limits where the fracture flow acts as an independent flow entity instead of being a part of porous matrix.

Although very wide in its scope, fluid flow studies in fractured media, as we have narrowed it down, deals exclusively with the study of this spontaneous phenomenon that helps displace oil out of matrix. This paper deals with quantifying, with the help of a numerical model, the experimental study of spontaneous imbibition process in both unfractured and fractured cores having negligible capillary pressure in the fracture.

The challenge associated with undertaking such experimental studies, on a laboratory scale, is that commercially available simulation softwares have some limitations. They are not designed for such a task. Out of the two popular softwares available to us, one has to have aquifer as a constant pressure boundary condition, whereas the other would not run without wells in place, thus undermining the spontaneity of the process of fluid flow. This made it amply clear to us that, if we had to understand the spontaneous imbibition process on the laboratory scale then, we would have to come up with our own numerical model which would have to be

flexible enough so that the affect of various parameters on spontaneous imbibition process can be studied in-depth. As a tool to verify this numerical model, we used X-Ray Tomography, as it is the best tool available to study fluid flow in porous media.

1.2 Principle of X-Ray Tomography

X-ray Computer Tomography (X-Ray CT) was introduced for medical purposes in the seventies and it was introduced for industrial purposes in the eighties. X-ray Tomography is a method of non-destructive testing (NDT). It is the imaging technique, similar to X-ray radiography; the only difference being the way X-ray radiation penetrates an object. **Fig. 1.1** shows the basic operation of X-ray CT. Here a digital detector or receptor replaces the X-ray film. The X-ray source, which emits a fan shaped beam, is then moved to different positions around the object. All the data generated, in each voxel, is then accumulated and processed with the help of a computer algorithm which generates a three dimensional CT image. The digital detector measures the linear attenuation coefficient, μ, the units of which are in form of dimensionless number called *Hounsfield unit*. The value of μ, depends on the density and the atomic composition of the matter in which X-ray propagates.

For a homogeneous object, the receptor reading, as per Huang[1], is given by:

$$I = I_0 e^{-\mu x} \qquad \ldots\ldots \quad (1)$$

Although slower than radiography, CT scanning is superior when it comes to revealing interior details of the imaged object. The scale of CT numbers, N_{CT}, has two fixed values independent of photon energy. For vacuum, air or body gas,

$$N_{CT} = -1000$$

and for water,

$$N_{CT} = 0.$$

The common method used for calculating porosity from CT images is:

$$\phi = \frac{N_{CT100\%Sat} - N_{CTDry}}{N_{CTWater} - N_{CTAir}} \qquad \ldots\ldots\ldots\ldots\ldots(2)$$

If water displaces air in the core, then saturation is given by:

$$S_w = \frac{N_{CTMat} - N_{CTDry}}{N_{CT100\%Sat} - N_{CTDry}} \qquad \ldots\ldots\ldots\ldots\ldots(3)$$

1.3 Mathematical Model

In order to form a mathematical model, we have to starts from the basic equations. For a one-dimensional two-phase system, such as oil-water system, the governing equations of fluid flow in porous media is given by Darcy's law:

Non-wetting phase: $$u_{nw} = -\frac{kk_{rnw}}{\mu_{nw}}\left(\frac{\partial p_{nw}}{\partial x} + g\rho_{nw}\sin\alpha\right) \quad \text{.....(4)}$$

Wetting phase: $$u_{w} = -\frac{kk_{rw}}{\mu_{w}}\left(\frac{\partial p_{w}}{\partial x} - g\rho_{w}\sin\alpha\right) \quad \text{.....(5)}$$

Here it is assumed that water is displacing oil. We use the capillary pressure equation:

$$P_c = p_{nw} - p_w \quad \text{.....(6)}$$

For counter-current imbibition we have,

$$u_w = -u_{nw} \quad \text{.....(7)}$$

Combining equation (4) – (7) and further reduction gives the following:

$$u_w\left(\frac{\mu_w k_{rnw} + \mu_{nw} k_{rw}}{kk_{rw}k_{rnw}}\right) = \left(\frac{\partial P_c}{\partial x}\right) + g(\rho_w - \rho_{nw})\sin\alpha \quad \text{.....(8)}$$

Again, for a given volume of porous medium, as per the law of conservation of mass, for a two-phase system having boundaries at x and $x + \Delta x$, we have:

$$q_{nw}\rho_{nw}\big|_x - q_{nw}\rho_{nw}\big|_{x+\Delta x} = A\phi\Delta x\frac{\partial}{\partial t}(S_{nw}\rho_{nw}) \quad \text{.....(9)}$$

$$q_{w}\rho_{w}\big|_x - q_{w}\rho_{w}\big|_{x+\Delta x} = A\phi\Delta x\frac{\partial}{\partial t}(S_{w}\rho_{w}) \quad \text{.....(10)}$$

Here it is assumed that the pore volume and fluid properties remain constant. This leads to cancellation of densities on both sides of the above two equations and expressing flow rate in terms of velocity, they reduce to:

$$\frac{\partial u_{nw}}{\partial x} + \phi\frac{\partial S_{nw}}{\partial t} = 0 \quad \text{.....(11)}$$

$$\frac{\partial u_w}{\partial x} + \phi \frac{\partial S_w}{\partial t} = 0 \qquad \text{…….....(12)}$$

For two-phase flow, we have:

$$S_{nw} = 1 - S_w \qquad \text{…....(13)}$$

and this implies:

$$\partial S_{nw} = -\partial S_w \qquad \text{…....(14)}$$

Thus combining equations (11) – (14) we have:

$$\frac{\partial u_{nw}}{\partial x} - \phi \frac{\partial S_w}{\partial t} = 0 \qquad \text{…….....(15)}$$

$$\frac{\partial u_w}{\partial x} + \phi \frac{\partial S_w}{\partial t} = 0 \qquad \text{…….....(16)}$$

Combining Darcy's law with the equations from law of conservation of mass and on reduction, we have:

$$\phi \frac{\partial S_w}{\partial t} = -\frac{\partial}{\partial x}\left[\frac{kk_{rw}k_{rnw}}{(\mu_w k_{rnw} + \mu_{nw} k_{rw})}\left(\left(\frac{dP_c}{dS_w}\right)\frac{\partial S_w}{\partial x}\right)\right] - \frac{\partial}{\partial x}\left[\frac{kk_{rw}k_{rnw}}{(\mu_w k_{rnw} + \mu_{nw} k_{rw})}\right] g\Delta\rho \sin\alpha$$

…….....(17)

which is the non-linear diffusion **saturation equation** and forms the basic equation of spontaneous imbibition. The first part of eqn. (17) is the diffusion term [*D*], which is determined by capillary forces whereas the latter, gravity term [*V*], is determined by the gravitational forces. For simplicity, eqn. (17) is written in the form:

$$\phi \frac{\partial S_w}{\partial t} = -\frac{\partial}{\partial x}\left[D\left(\frac{\partial S_w}{\partial x}\right)\right] - \frac{\partial}{\partial x}[V]\Delta\rho \sin\alpha \qquad \text{…….....(18)}$$

where,

$$[D] = \left[\frac{kk_{rw}k_{rnw}}{(\mu_w k_{rnw} + \mu_{nw} k_{rw})}\left(\frac{dP_c}{dS_w}\right)\right] \qquad \text{…….....(19)}$$

$$[V] = \left[\frac{kk_{rw}k_{rnw}}{(\mu_w k_{rnw} + \mu_{nw} k_{rw})}\right] g \qquad \text{…….....(20)}$$

Extending this from a one-dimensional to two-dimensional form we have the general form of eqn. (18) as:

$$\phi \frac{\partial S_w}{\partial t} = -\frac{\partial}{\partial x}\left[D\left(\frac{\partial S_w}{\partial x} \right)\right] - \frac{\partial}{\partial y}\left[D\left(\frac{\partial S_w}{\partial y} \right)\right] - \frac{\partial}{\partial x}[V]\Delta\rho \sin\alpha - \frac{\partial}{\partial y}[V]\Delta\rho \sin\alpha$$

…….(21)

1.4 Finite Difference Numerical Model

In order to arrive at a solution of eqn. (21), we have to solve the equation numerically. The most common of the assumptions is to assume the effect of gravity to be small and hence neglected. Also, if the non-wetting phase is assumed to be air, then mobility of air is much higher than mobility of water and the mobility ratio water to air is almost zero. This simplifies the eqn. (21) to:

$$\phi \frac{\partial S_w}{\partial t} = -\frac{\partial}{\partial x}\left[D\left(\frac{\partial S_w}{\partial x} \right)\right] - \frac{\partial}{\partial y}\left[D\left(\frac{\partial S_w}{\partial y} \right)\right] \qquad \text{…….(22)}$$

and its finite difference equivalent, central difference in space and forward difference in time, is given by:

$$\frac{D^n_{i-\frac{1}{2},j}}{\Delta x_{i-\frac{1}{2},j}} \frac{\left((S_w)^{n+1}_{i-1,j} - (S_w)^{n+1}_{i,j}\right)}{\Delta x_{i,j}} + \frac{D^n_{i+\frac{1}{2},j}}{\Delta x_{i+\frac{1}{2},j}} \frac{\left((S_w)^{n+1}_{i+1,j} - (S_w)^{n+1}_{i,j}\right)}{\Delta x_{i,j}}$$

$$+ \frac{D^n_{i,j-\frac{1}{2}}}{\Delta x_{i,j-\frac{1}{2}}} \frac{\left((S_w)^{n+1}_{i,j-1} - (S_w)^{n+1}_{i,j}\right)}{\Delta x_{i,j}} + \frac{D^n_{i,j+\frac{1}{2}}}{\Delta x_{i,j+\frac{1}{2}}} \frac{\left((S_w)^{n+1}_{i,j+1} - (S_w)^{n+1}_{i,j}\right)}{\Delta x_{i,j}} = -\phi_{i,j} \frac{\left((S_w)^{n+1}_{i,j} - (S_w)^{n}_{i,j}\right)}{\Delta t}$$

…….(23)

where following the discretization process the diffusion term is calculated, for example, at the face of the grid block as:

$$D_{i-\frac{1}{2},j} = \frac{(k_w)_{i-\frac{1}{2},j}}{\mu_w} \left(\frac{dP_c}{dS_w} \right)_{i-\frac{1}{2},j} \qquad \text{…….(24)}$$

The capillary pressure term is calculated as:

$$\left(\frac{dP_c}{dS_w} \right)_{i-\frac{1}{2},j} \approx \left(\frac{P_c(S_w + \Delta S) - P_c(S_w)}{\Delta S} \right)_{i-1,j} \qquad \text{…….(25)}$$

and the distance to one of the faces of the grid block with respect to center is given by:

$$\Delta x_{i-\frac{1}{2},j} = \Delta x_{i,j} - \Delta x_{i-1,j} \qquad \text{…….(26)}$$

In eqn. (24) the magnitude of the relative permeability is governed by the upstream value whereas the absolute permeability at the face is taken as the harmonic average of the two different absolute permeability values across the face. With the help of eqn. (23) a numerical code is generated, which is flexible enough to take into account various desired boundary conditions.

1.5 Theoretical Background and Verification Tasks

1.5.1 Handy's[2] Experiment of Spontaneous Imbibition

Eqn. (22) has been used by many researchers such as Babadagli and Ershaghi[4], Li and Horne[5], etc. to describe spontaneous imbibition. One of the earliest attempts with air-water system was made by Handy[2] who assumed that the capillary term varied linearly with distance. This is true as long as we assume a piston type displacement of the non-wetting phase by the wetting phase and the potential, generated by the capillary forces, provides the driving force. With these assumptions, eqn. (22) for cylindrical cores reduces to the following form:

$$Q_w^2 = \left(\frac{2P_c k_w \phi A^2 S_w}{\mu_w} \right) t \qquad \text{…….(27)}$$

This is the equation of a line and on a plot of squared of the water imbibed versus time, will pass through the origin.

We chose Handy's data to verify our numerical code. The reason for doing this is to prove that our simulator could exactly match that data as well as bring forth the limitation of the initial assumption that capillary pressure varies linearly with distance. This is true for early time but the relationship breaks down as time progresses. If imbibition is allowed to prolong into late time, it levels off and stops. This is shown in **Fig. 1.2,** which shows the results of our numerical simulation run. We plotted one of the outputs of our simulator, a plot of capillary pressure versus distance and as it is clear from **Fig. 1.3**, the relationship is a not a linear one.

1.5.2 Spontaneous Imbibition Experiment of Unfractured Core

Garg *et al*[3] solved eqn. (21) for one-dimensional saturation data measured with the help of X-ray CT. They setup a mechanism with which they could simultaneously measure the weight of the water imbibed and measure the water saturation with the help of CT scanner. We chose to compare the validity of our code with the help of two simultaneously varying data, the first being weight gain of the imbibed water expressed as a fraction of total water imbibed and the other being water saturation measured with X-ray CT scanner. As is with all multiple parameters, a match with one does not necessarily guarantee match with the other and this leads to lot of iterative effort before both can be matched. The out of the two, the data collected for weight gain was a tricky one as, at the initial stages, buoyancy forces had to be contended with as it does not start from the origin. We started with a power expression for relative permeability and found that an exponent of n = 8.5, gave us a close match as can be seen in **Fig. 1.4**. Next we varied the different values of end-point relative permeability to arrive at an adequate match for saturation. We found that this value had more sensitive to saturation than the amount of water imbibed, which was almost the same in all cases of different exponents. **Figs. 1.5** and **1.6** shows the effect of various values of saturation exponent and **Figs. 1.7** and **1.8** gives shows the effect of various values of end-point relative permeability values. Hence:

$$k_{rw} = 0.045 S_w^{8.5} \qquad \text{…….(28)}$$

We used a variable capillary pressure curve as shown in **Fig. 1.9** as input. We also did the sensitivity study on gridblock size and the time steps used in the simulation and found that 15 gridblocks and time step of 2 seconds were enough to adequately run our model. The output from the code can track the saturation front in one-dimension as shown in **Fig. 1.10**, where saturation for each grid block in a section are plotted. There is a difference in methodologies between our experimental study and experimental work conducted by Garg *et al*[3]. They used the following logarithmic capillary pressure relation:

$$P_c = P_c^o \ln S \qquad \text{…….(29)}$$

where P_c^o is the threshold capillary pressure and S is the normalized saturation. They have used a power expression for air-water relative permeability as given by:

$$k_{rw} = k_{rw}^o S^n, \qquad n \geq 1 \qquad \text{…….(30)}$$

Again k_{rw}^o is the end point relative permeability and they matched the experimental data with n = 2.5. We have gone further than this and our code can incorporate a variable capillary pressure data and a variable relative permeability data even though we have used a similar kind of relationship.

The departure from the experimental data initially, in **Figs. 1.6** and **1.8**, is on account of high imbibition rate. The anomaly at the top of the core, we believe, is due to diffraction of X-rays which produces artifacts, areas of high CT numbers. The sides of the core were covered by epoxy and hence shielded from this effect.

Summarily, we matched the weight gain and CT water saturation using the following parameters:

Garg *et al*[3] have incorporated the effect of gravity which we have neglected due to the small size of the core. We had to alter horizontal permeability as well, at normalized height of 0.6 to 80 md so as to match the experimental results at 360 seconds. Having matched the one-dimensional data, we went ahead and compared the two-dimensional saturation front pictures with our simulator output. Here also we got an adequate match on a picture-by-picture basis, as shown in **Fig. 1.11**. To the left are the pictures appearing in Garg *et al*[3] paper and to the right are our simulator results.

1.5.3 Spontaneous Imbibition Experiments with Fractured Core

We also carried out our own experiments with fractured Berea core. The aim was to again put to test the validity of the code and for its faithful reproduction of the experiment. For the experiment we used Berea core, 1.5 inches in diameter and 2.5 inches in height with an average permeability of around 200 md. It was first dried for 24 hours and then put in a water bath at the beginning of the experiment. Great care was taken so that the constant level of water was maintained at the bottom. The experiment was conducted at room temperature and normal tap water was used in the water bath. As can be seen from **Fig. 1.12**, as soon as experiment was started the clock reported the actual time of the experiment. It took close to half an hour for the imbibition saturation front to travel from bottom to top. Initially, CT images

were taken at one-minute time interval subsequently to be increased near the end of the experiment, as shown in **Fig. 1.12**. The energy level used in the scanning process was 120 keV that gave us the best resolution. The step-by-step match is shown in **Fig. 1.13**. The obvious point to be noticed here is that both **Figs. 1.12** and **1.13** have the same number of time steps. Once again we used a variable capillary pressure curve and a variable relative permeability curve and obtained an adequate match.

1.6 Conclusions

Our aim in this paper was to start from basics and come up with a robust two-dimensional two-phase numerical model for spontaneous imbibition that could faithfully reproduce laboratory experiments. This model was rigorously verified by experimental data. With this model we have successfully accomplished the following three experimental objectives:

1. Validated the experimental data of Handy and proved the limitations of the most common assumption used to solve eqn. (22) analytically.

2. Matched the results of Garg *et al*[3] X-ray CT experiment, with two simultaneously varying parameters of weight gain and water saturation.

3. Reproduced accurately our own experiment of a fractured core.

With this numerical model we will extend this numerical model to study of capillary pressure and relative permeability during spontaneous imbibition, on a more detailed basis, for oil-water system.

1.7 Nomenclature

I_0 = Receptor reading without the object

μ = Linear attenuation coefficient for the object

x = Object thickness along the path of that ray

$N_{CT100\%Sat}$ = CT number of 100% saturated voxel

N_{CTDry} = CT number of dry voxel

$N_{CTWater}$ = CT number of Water = 0.0

N_{CTAir} =CT number of Air = -1000.0

N_{CTMat} = CT number of the matrix

ϕ = Porosity of the matrix

S_{nw} = Saturation of non-wetting phase

S_w = Saturation of wetting phase

u_{nw} = Velocity of non-wetting phase

u_w = Velocity of wetting phase

μ_{nw} = Viscosity of non-wetting phase

μ_w = Viscosity of wetting phase

k = Absolute permeability of rock

k_{rnw} = Viscosity of non-wetting phase

k_{rw} = Viscosity of wetting phase

p_{nw} = pressure of non-wetting phase

p_w = Pressure of wetting phase

ρ_{nw} = Density of non-wetting phase

ρ_w = Density of wetting phase

g = Acceleration due to gravity

α = Angle, measured counter-clockwise, with the horizontal

P_c = Capillary Pressure

q_{nw} = Flow-rate of non-wetting phase

q_w = Flow-rate of wetting phase

A = Area of control volume in eqn. (9) and (10) / Area of core in eqn. (27)

x, y = Linear dimensions along principal axes

i,j = Grid block directions along principal axes

n = Time step number

ΔS = Change of Saturation of wetting phase

1.8 References

1. Huang, H.K., *Elements of digital radiology: A professional handbook and guide*, Prentice-Hall, New Jersey (1987).

2. Handy, L.L.: "Determination of Effective Capillary Pressures for Porous Media from Imbibition Data," Petroleum Transactions AIME, Vol. 219, 1960, 75-80.

3. Garg, A., Zwahlen, E. and Patzek, T.W.: "Experimental and Numerical Studies of One-Dimensional Imbibition in Berea Sandstone," paper presented at the 16th Annual American Geophysical Union Hydrology Days, Fort Collins, Colorado, 15-18 Apr, 1996.

4. Babadagli, T. and Ershaghi, I.: “Imbibition Assisted Two-Phase Flow in Natural Fractures,” paper SPE 24044 presented at the 1992 SPE Western Regional Meeting, Bakersfield, California, Mar 30-Apr 1.

5. Li, K. and Horne, R.N.: “Characterization of Spontaneous Water Imbibition into Gas-Saturated Rocks,” paper SPE 62552 presented at the 2000 SPE/AAPG Western Regional Meeting, Long Beach, California, 19-23 June.

6. Akin, S. and Kovscek, A.R.: “Imbibition Studies of Low-Permeability Porous Media,” paper SPE 54590 presented at the 1999 SPE Western Regional Meeting, Anchorage, Alaska, 26-27 May.

7. Reis, J.C. and Cil, M.: “A Model for Oil Expulsion by Counter-Current Water Imbibition into Gas-Saturated Matrix Blocks,” J. Pet. Sci. & Eng., **10**: 97-107.

8. Zhou, D., Kamath, J., and Kovscek, A. R.: “An Investigation of Counter-Current Imbibition Process in Diatomite,” Paper SPE 68837 presented at the 2001 SPE Western Regional Meeting, Bakersfield, California, 26-30 Mar.

Table 1.1 – Summary of key parameter used to match CT water saturation

Parameters	Value
k	300 md
$k_{rw}^{\ o}$	0.045
$P_c^{\ o}$	2.5 psi
ϕ	0.22
n	0.5
S_{wi}	0.1

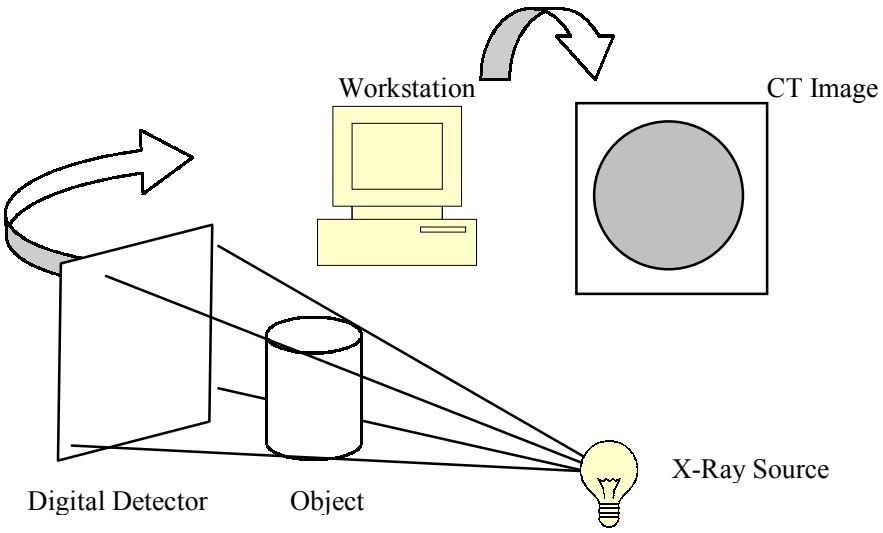

Fig. 1.1 – Conceptual representation X-Ray Tomography

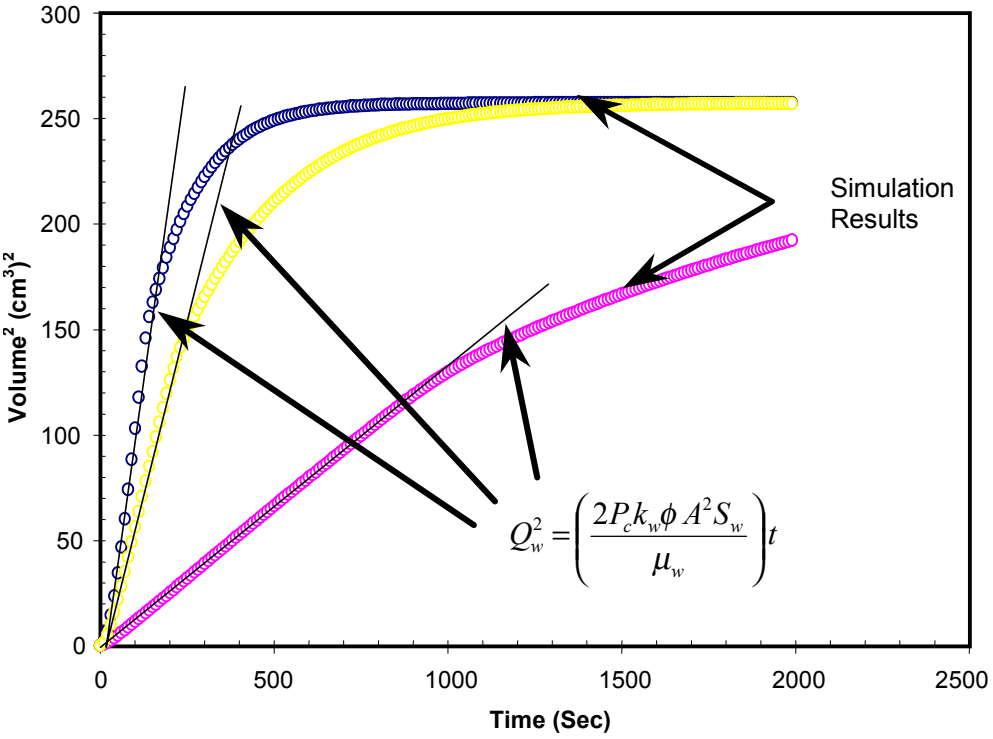

Fig. 1.2 – Comparison of Handy's data with numerical simulation

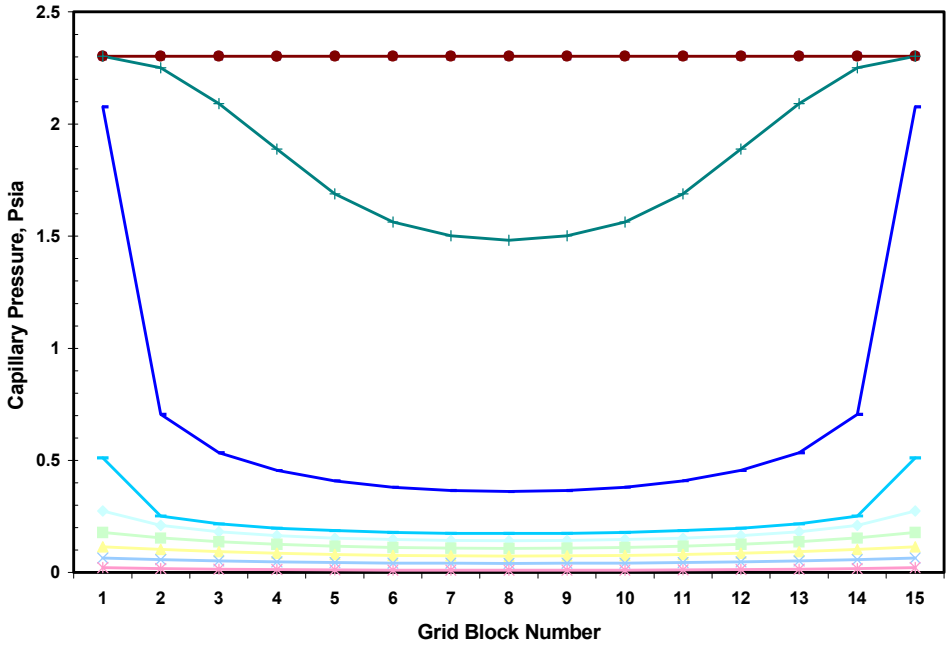

Fig. 1.3 – Capillary pressure versus distance

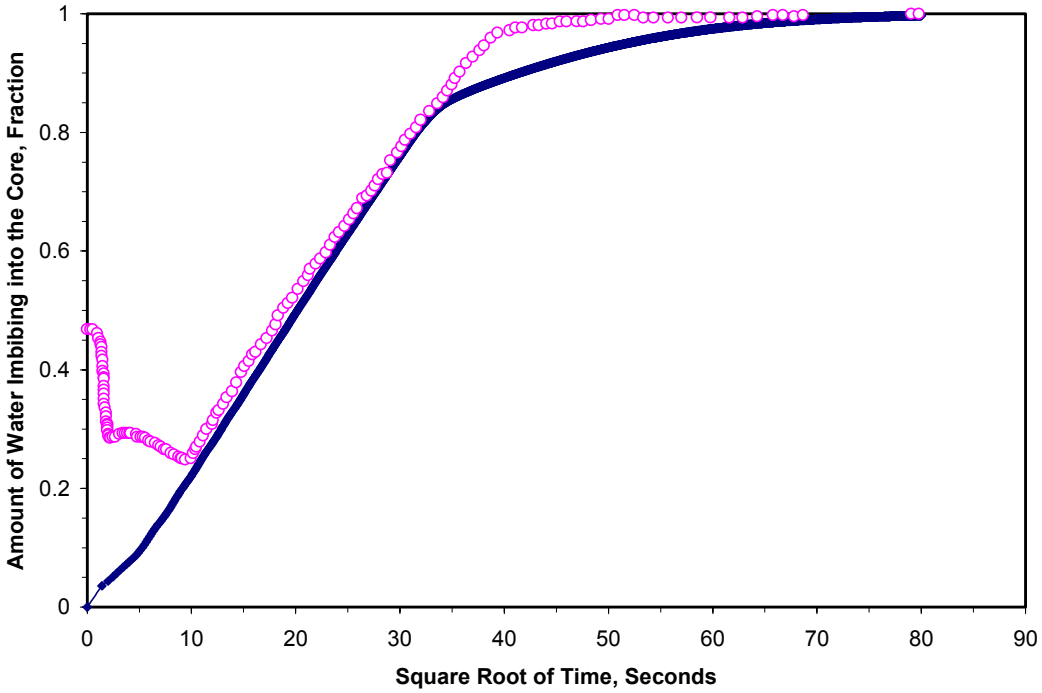

Fig. 1.4 – Weight gain versus square root of imbibition time

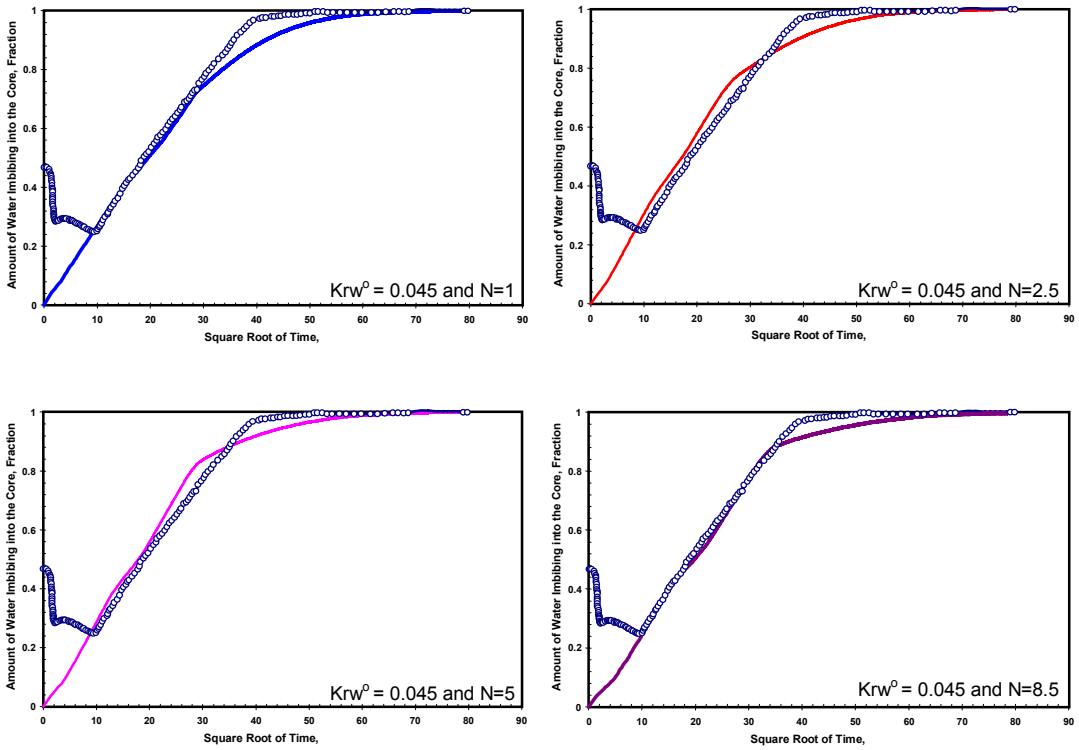

Fig. 1.5 – Sensitivity study on weight gain data at constant end-point saturation

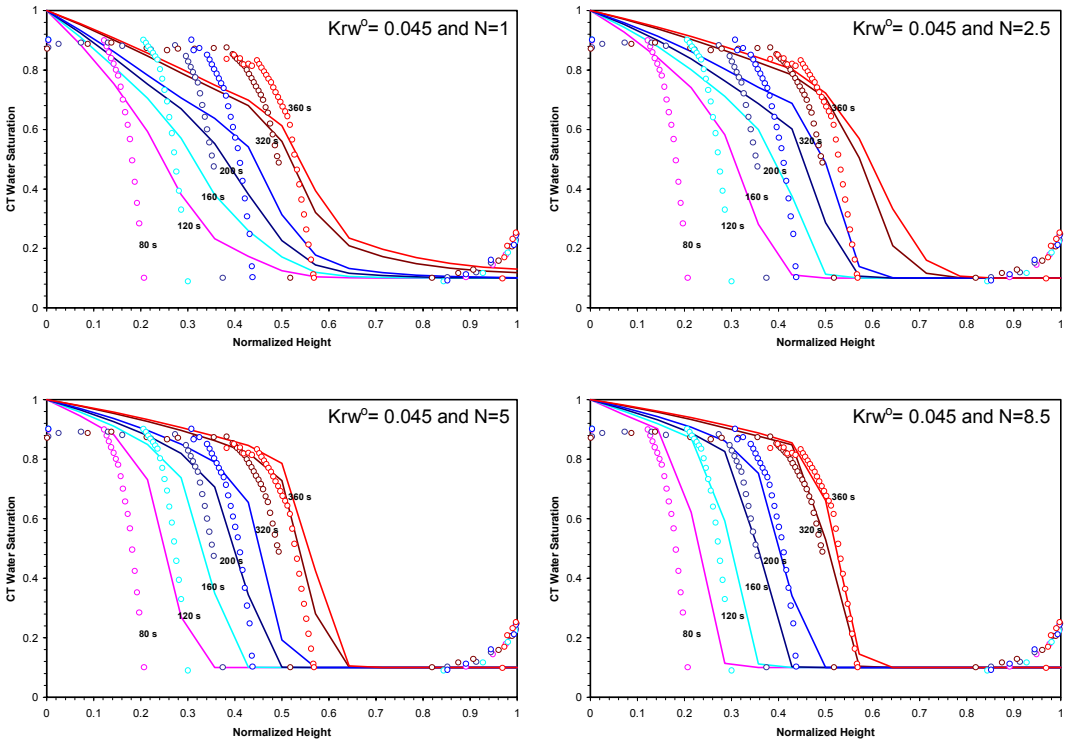

Fig. 1.6 – Sensitivity study on saturation data at constant end-point saturation

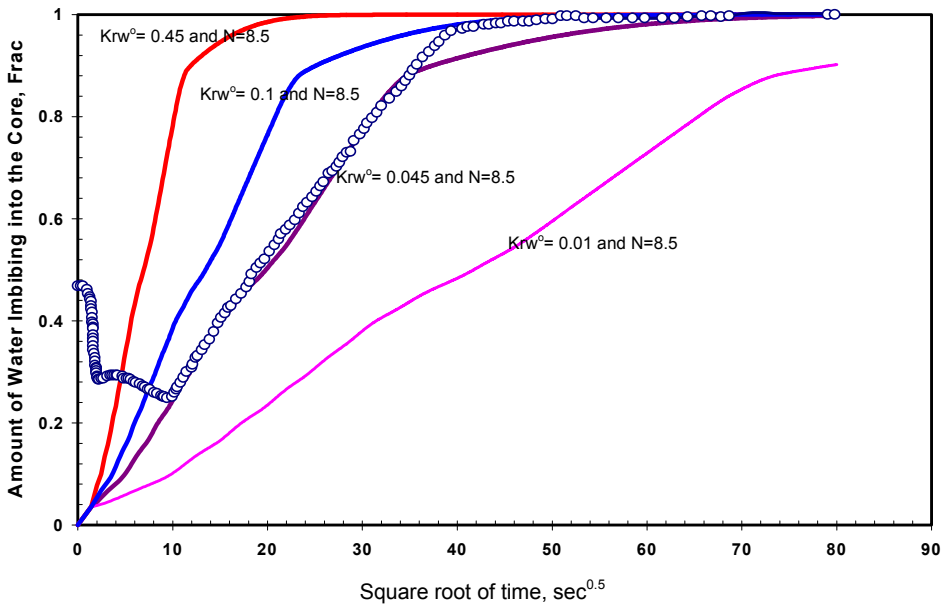

Fig. 1.7 – Sensitivity study on weight gain data at constant saturation exponent

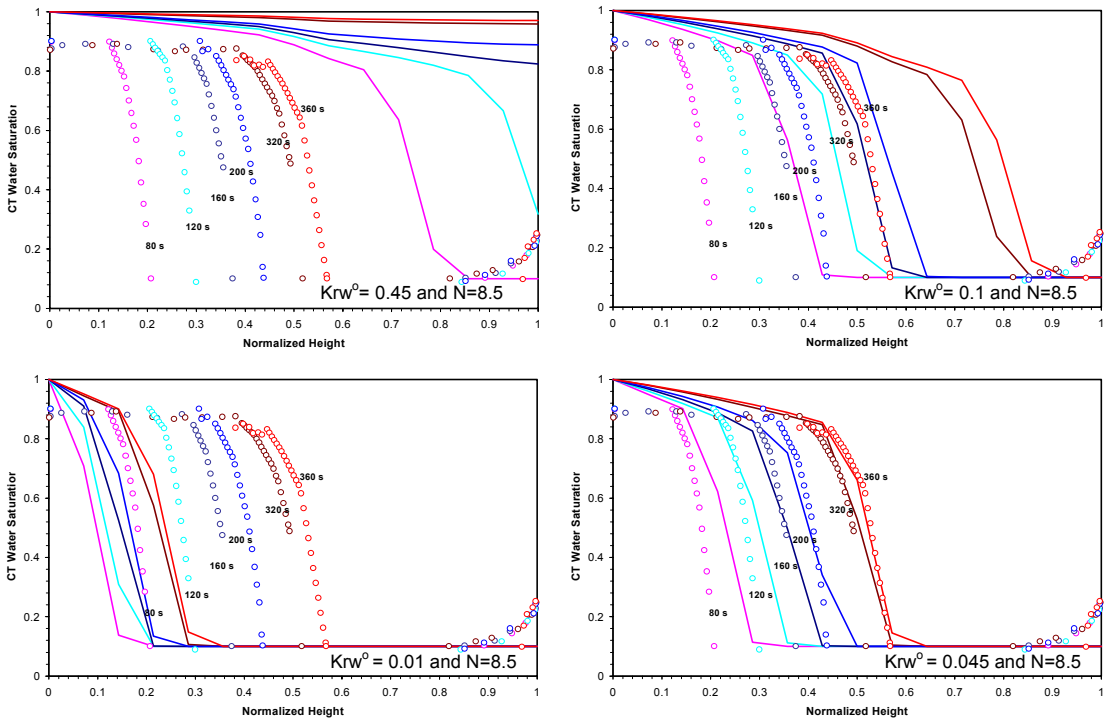

Fig. 1.8 – Sensitivity study on saturation data constant saturation exponent

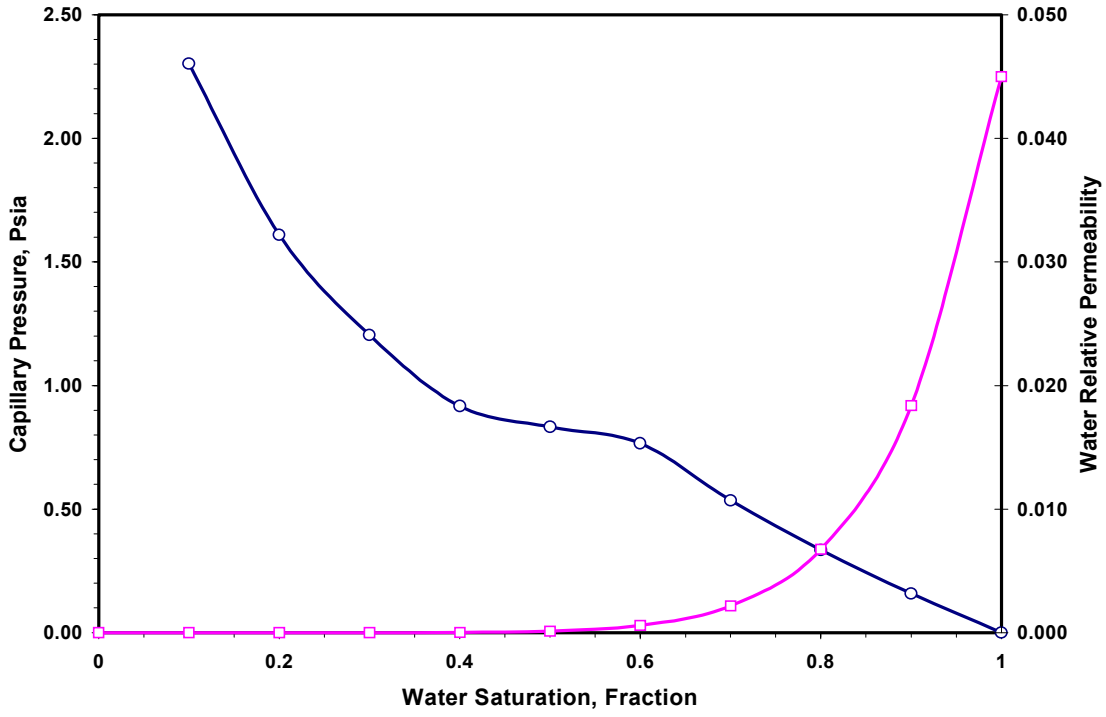

Fig. 1.9 – Final capillary pressure and relative permeability data used in simulation

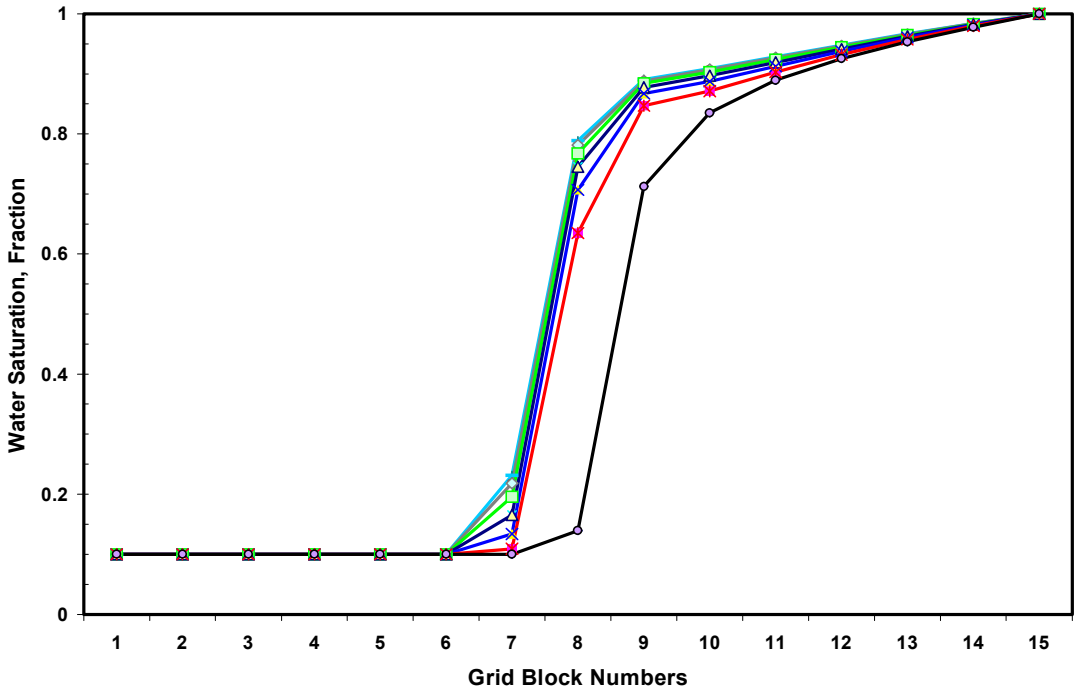

Fig. 1.10 – Saturation versus distance (front is moving from left to right)

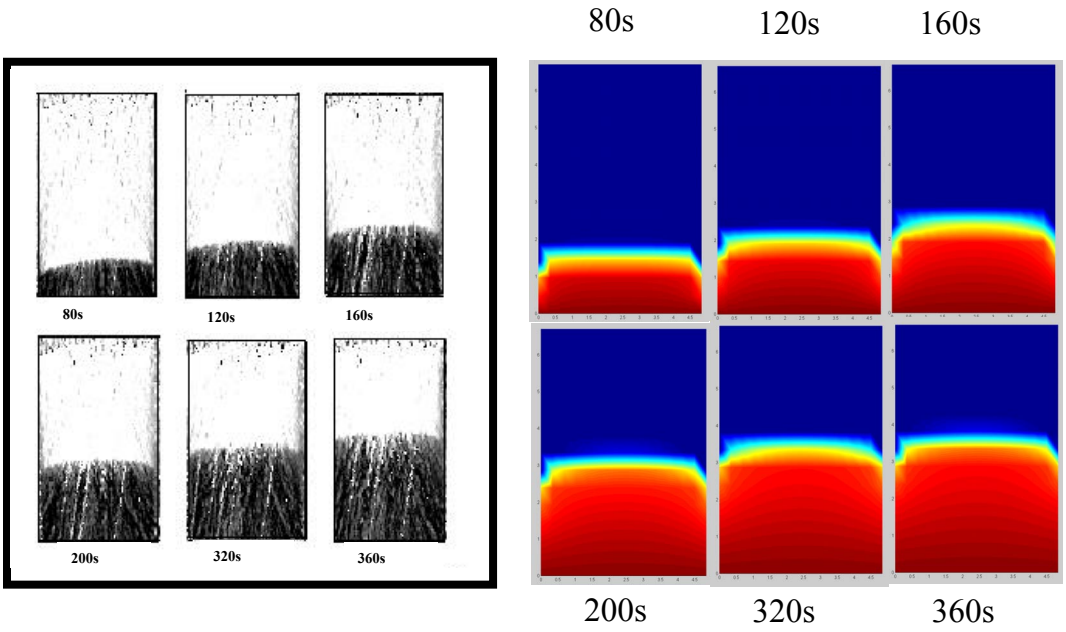

Fig. 1.11 – Two-dimensional CT water saturation front movement

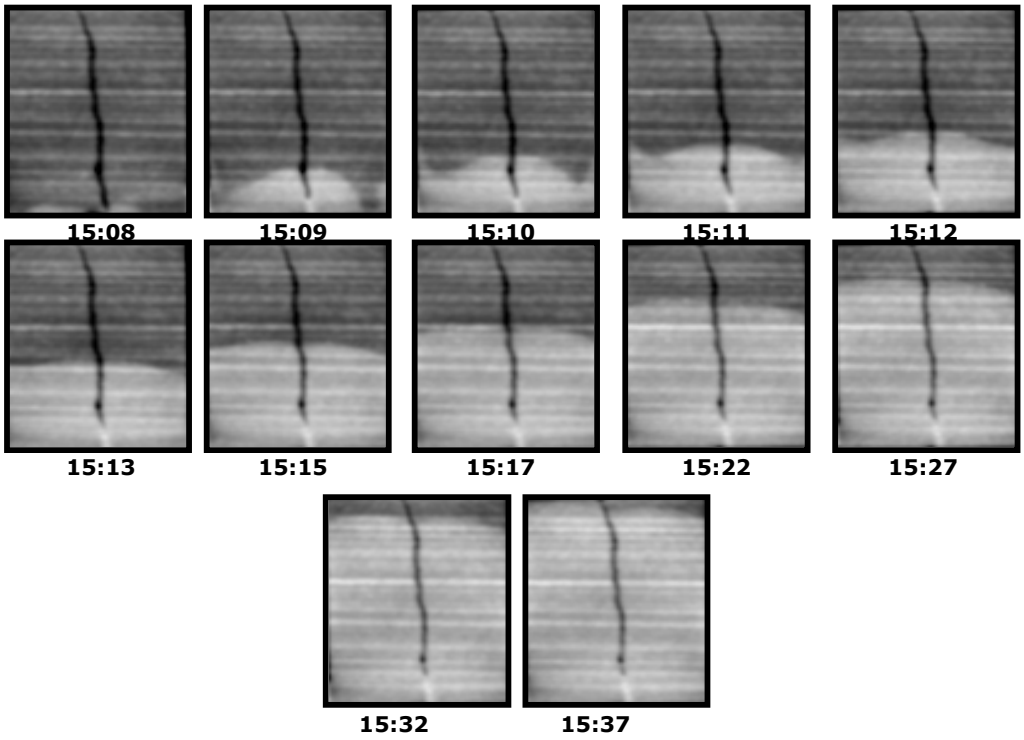

Fig. 1.12 – Two-dimensional CT water saturation front movement in fractured core

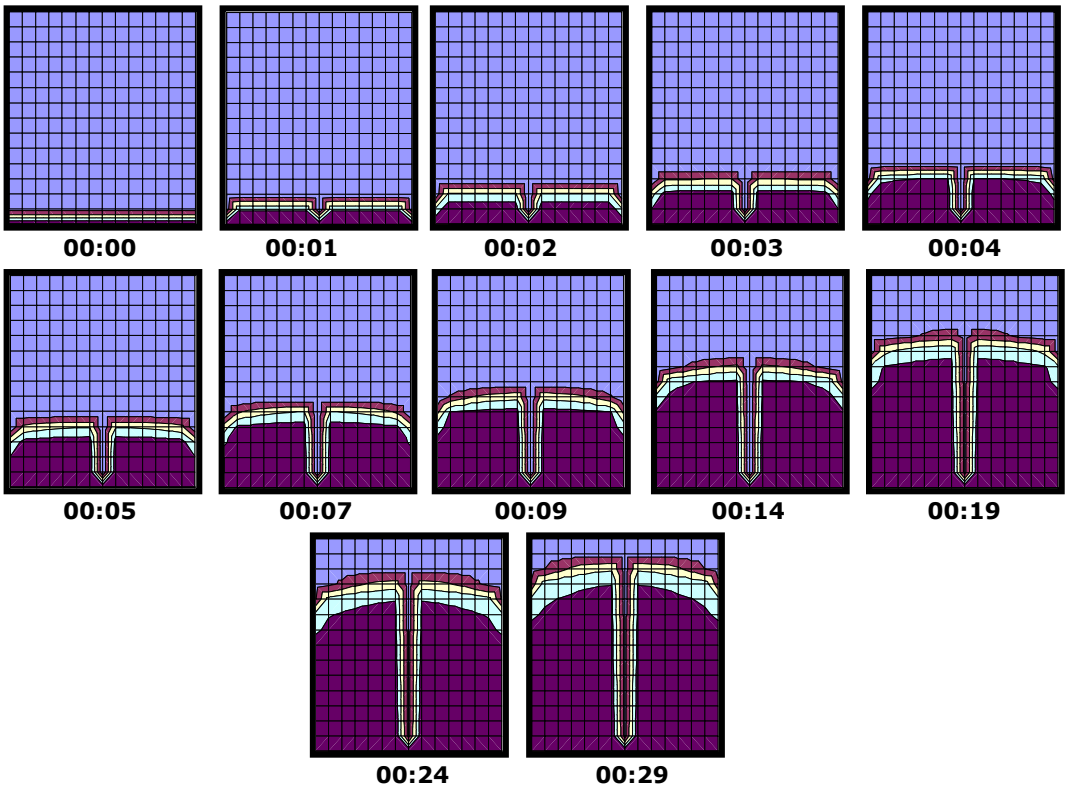

Fig. 1.13 – Two-dimensional simulation water saturation front movement